

Qudit Implementation of the Rodeo Algorithm for Quantum Spectral Filtering

J. C. S. Rocha*

Departamento de Física, Universidade Federal de Ouro Preto - UFOP, Ouro Preto, Minas Gerais, Brasil.

R. A. Dias†

Departamento de Física, Universidade Federal de Juiz de Fora - UFJF, Minas Gerais, Brasil.

(Dated: March 18, 2026)

Qudits, the multi-level generalization of qubits, provide a natural extension of the binary paradigm in quantum computation and offer new opportunities to enhance algorithmic performance. Beyond their direct applicability to the simulation of multi-level quantum systems, higher-dimensional ancillae can improve sampling efficiency in quantum algorithms by enabling the simultaneous implementation of multiple control operations, thereby reducing circuit complexity. In this work, we pursue three main objectives. First, we present a formulation of the Rodeo algorithm employing a general d -level ancilla qudit. Second, we introduce the concept of the *Rodeo kernel*, defined as a two-frequency interferometer, which acts as a spectral filter in the energy domain. Finally, we propose a microcanonical protocol for the Rodeo algorithm. This protocol enables the estimation of entropic quantities through a single energy sweep and admits a natural interpretation as a Gaussian convolution of the density of states. To support the theoretical analysis, we perform numerical evaluations of the corresponding quantum circuit using ancilla qudits of dimensions three, four, and five. The simulations are performed for the one-dimensional Ising model, considering both spin- $1/2$ and spin-1 particles. The ancilla qutrit implementation exhibits an 18% reduction in fluctuations compared to the qubit implementation. Our results show that the qudits provide a framework for spectral analysis and thermodynamic characterization of multi-level quantum systems.

Keywords: Quantum Computing, Rodeo Algorithm, Qudit, Qutrit, Entropy

I. INTRODUCTION

In the early 1980s, Richard Feynman argued that quantum computers can achieve exponential speedups for certain problems by exploiting the exponentially large structure of Hilbert space [1]. Shortly thereafter, David Deutsch formalized the notion of a universal quantum computer and demonstrated that classical devices cannot efficiently simulate general quantum systems, thereby establishing the distinctive computational power of quantum mechanics [2].

Within this framework, the qudit—a multi-level quantum computational unit [3–5]—can surpass the conventional two-level qubit in both aspects. It provides a natural platform for simulating multi-level quantum systems and can enhance algorithmic efficiency. In particular, qudits enable an intrinsically parallel architecture by allowing the simultaneous implementation of multiple control operations, while offering an enlarged state space for information storage and processing. These features can reduce circuit complexity. Although maintaining high fidelity in multi-tone control is challenging, experimental realization on 5- and 8-level qudits in a trapped-ion system demonstrates competitive performance in implementing Grover’s algorithm [6]. Coherent control of 10-level qudits has been demonstrated in optical platforms [7]. Furthermore, solid-state devices also constitute a hardware platform for the implementation of multi-level qudit systems [8].

Inspired by recent implementation of Ramsey interferometry in multi-level quantum systems [9, 10], and motivated by its close conceptual relationship with the Rodeo algorithm [11–13], we formulate the Rodeo algorithm within a general d -dimension qudit framework. In the Ramsey spectroscopy, a coherent superposition of internal states accumulates relative phases during a period of free evolution. In the Rodeo algorithm, this free-evolution arm is effectively realized by a controlled operator followed by a phase shift, see FIG. 1. In both settings, the d -dimensional quantum Fourier transform (QFT) [14] naturally generalizes the role of the Hadamard gate used in qubit-based architecture. Beyond that, the Rodeo protocol requires access to a sufficiently general set of multi-level quantum gates [15–19]. As all required tools are currently available, the proposed approach is readily implementable.

* jcsrocha@ufop.edu.br

† rodrigo.dias@ufjf.br

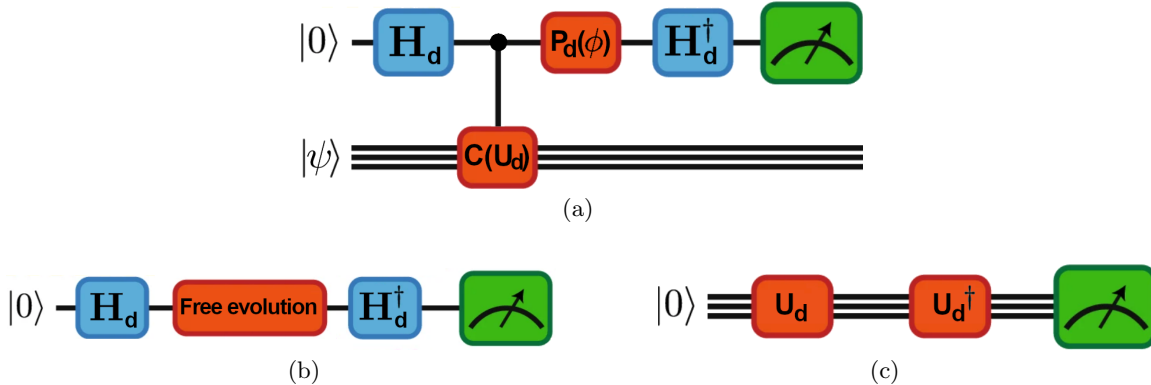


FIG. 1. (Color online) Circuit diagrams illustrating (a) the Rodeo algorithm, (b) a Ramsey interferometer, and (c) a Loschmidt-echo protocol. In the Rodeo implementation, the free-evolution arm of the Ramsey interferometer is replaced by a controlled time-evolution operator followed by a phase shift. As the phase shift constitutes an attempt to reverse the effect of the controlled evolution on the ancilla qudit, the Rodeo circuit admits a natural interpretation in terms of a Loschmidt echo.

In the Rodeo protocol, the phase shift is introduced as a tentative attempt to invert the effect of the controlled operation on the ancilla qudit, thereby allowing a natural interpretation in terms of the Loschmidt echo. In this context, if quantum dynamics were perfectly reversible, a quantum state evolved forward in time would return exactly to its initial configuration upon a time-reversal operation. In simple words, the Loschmidt echo quantifies the survival ratio of a state under forward and backward evolution. Importantly, beyond serving as a measure of reversibility, the temporal dependence of the Loschmidt echo encodes the energy distribution associated with the initial state. In the Rodeo algorithm, this connection underlies the extraction of spectral information from time-domain interference measurements. We also introduce a single-input protocol that enables estimation of the density of states and microcanonical entropy using the Rodeo algorithm. This protocol is based on the convolution of a Fourier series with a Gaussian distribution. The resulting signal serves as a Gaussian smoothing filter applied to the quantum spectrum.

This paper is organized as follows. In Sec. II, we present the theoretical framework of the algorithm. In particular, Sec. II A revisits the Rodeo algorithm and describes its implementation in qudit systems through the step-by-step evolution of the joint ancilla–system state. In Sec. II A 4, we show how the width of the success-probability peak decreases as the ancilla dimension increases. In Sec. II B, we derive the Rodeo kernel through a Fourier-series expansion, showing that a small-amplitude high-frequency harmonic perturbation can produce a noise reduction, more pronounced for the ancilla qutrit implementation, while simultaneously improving spectral resolution. In this section, we also discuss the connection with the Loschmidt amplitude. In section II C we introduce the microcanonical ensemble protocol for entropy estimation, which interprets the Rodeo algorithm as a convolution-based spectral smoothing filter. Section III presents the numerical evaluation of the proposed approach for the one-dimensional Ising model. Specifically, in Sec. III A, we consider spin- $1/2$ particles and compare the qubit and qudit implementations, finding excellent agreement with the theoretical predictions. In Sec. III B, we study the spin-1 Ising model and show that the method accurately reproduces the quantum degeneracy of the system. Finally, the conclusions and perspectives are presented in Sec. IV.

II. THEORETICAL FRAMEWORK

We initiate the formal treatment by revisiting the Rodeo algorithm and explicitly extending its framework to qudit architectures through a detailed derivation of the evolution of the joint ancilla–system quantum state across the full quantum circuit.

A. Revisiting the Rodeo algorithm

1. Initialization

Let \mathcal{H} be a finite-dimensional Hamiltonian with spectral decomposition

$$\mathcal{H}|x\rangle = E_x|x\rangle, \quad (1)$$

where $\{|x\rangle\}$ denotes the complete set of orthonormal energy eigenstates. Each eigenstate $|x\rangle$ is encoded in a tensor product of k qudits, sufficient to represent any physically accessible state of the system under consideration. For a system composed of d' -level particles, d' -dimensional qudits constitute a natural — though not unique — choice of encoding. Under this correspondence, the number of qudits is equal to the number of particles, N . Hence, in the following, we set $k = N$. A general pure system state can therefore be expressed as

$$|\psi\rangle = \sum_{x=0}^{d'^N-1} c_x |x\rangle, \quad \text{where } c_x = \langle x|\psi\rangle, \quad (2)$$

for notational simplicity, the summation limits of the system basis states will be omitted in the following expressions.

We introduce an ancilla qudit of dimension d , with computational basis $\{|\ell\rangle\}_{\ell=0}^{d-1}$. In general, for heterogeneous hardware architectures, the dimensions d and d' need not coincide. Let us assume that ancilla is initialized in $|0\rangle$. Then the joint initial state is considered to be

$$|\Psi_0\rangle = |0\rangle \otimes |\psi\rangle = \sum_x c_x |0\rangle \otimes |x\rangle. \quad (3)$$

The first step is to prepare the ancilla qudit in the uniform superposition state

$$|+\rangle_d = \frac{1}{\sqrt{d}} \sum_{\ell=0}^{d-1} |\ell\rangle, \quad (4)$$

which can be done by applying the d -dimensional quantum Fourier transform (QFT)[20] to the state $|0\rangle$, namely $|+\rangle_d = \mathbf{H}_d|0\rangle$, where

$$\mathbf{H}_d = \frac{1}{\sqrt{d}} \sum_{\ell, n=0}^{d-1} \omega^{\ell n} |\ell\rangle\langle n|, \quad \text{with } \omega = e^{i2\pi/d}. \quad (5)$$

The resulting joint state is

$$|\Psi_1\rangle = |+\rangle_d \otimes |\psi\rangle = (\mathbf{H}_d \otimes \mathbf{1}_{d'}^{\otimes N}) |\Psi_0\rangle, \quad (6)$$

$$= \frac{1}{\sqrt{d}} \sum_{\ell=0}^{d-1} \sum_x c_x |\ell\rangle \otimes |x\rangle, \quad (7)$$

where

$$\mathbf{1}_{d'} = \sum_{q=0}^{d'-1} |q\rangle\langle q|, \quad (8)$$

denotes the identity operator acting on a single system qudit. Since $|x\rangle$ is a tensorial product of N qudits then $\mathbf{1}_d^{\otimes N} |x\rangle = |x\rangle$.

2. Loschmidt echo-like circuit

Following the Rodeo circuit, we apply a controlled unitary operation, defined as

$$C(U_{d'}) = \sum_{n=0}^{d-1} |n\rangle\langle n| \otimes (U_{d'})^n. \quad (9)$$

Although the Rodeo algorithm applies to arbitrary unitary observables, here we focus on solving the time-independent Schrödinger equation. Accordingly, we choose $U_{d'}$ to be the time-evolution operator

$$U_{d'} = e^{-i\mathcal{H}t}. \quad (10)$$

Notably, we adopt units such that $\hbar = 1$. In the original formulation of the Rodeo algorithm, the evolution time t is sampled from a Gaussian distribution. Nevertheless, alternative distributions are possible, including those defined by adaptive parametrization schemes. Recent results indicate that sampling t according to a geometric series leads to improved sampling performance [21]. Applying the controlled evolution to the joint state $|\Psi_1\rangle$ yields

$$\begin{aligned} |\Psi_2\rangle &= C(U_{d'}) |\Psi_1\rangle \\ &= \frac{1}{\sqrt{d}} \sum_{\ell=0}^{d-1} \sum_x c_x e^{-iE_x t \ell} |\ell\rangle \otimes |x\rangle, \end{aligned} \quad (11)$$

where we have used the orthonormality of the computational basis. The next step is to apply a phase-shift operation to the ancilla qudit. The phase shift operator is

$$P_d(\phi) = \sum_{n=0}^{d-1} \omega^{\phi n/\pi} |n\rangle\langle n|, \quad (12)$$

where $\omega = e^{i2\pi/d}$, as defined in Ref.[22]. When the system state coincides with an eigenstate of the Hamiltonian, $|\psi\rangle = |x\rangle$, an appropriate choice of the phase parameter ϕ can reverse the effect of the controlled time-evolution operator. In practice, this phase is chosen as a trial value, which we parametrize as

$$\phi = \frac{Ed}{2}t, \quad (13)$$

where E is interpreted as a trial eigenvalue associated with the target eigenstate, and t denotes the evolution time defined in eqn (10).

Since the phase shift acts exclusively on the ancilla qudit, the resulting joint state is

$$\begin{aligned} |\Psi_3\rangle &= \left[P_d(\phi) \otimes \mathbb{1}_{d'}^{\otimes N} \right] |\Psi_2\rangle \\ &= \frac{1}{\sqrt{d}} \sum_{\ell=0}^{d-1} \sum_x c_x e^{-i\omega_x t \ell} |\ell\rangle \otimes |x\rangle. \end{aligned} \quad (14)$$

where $\omega_x = E_x - E$.

3. Final state

The next step of the circuit consists of a basis transformation on the ancilla qudit, returning it from the Fourier basis to the computational basis. This is achieved by applying the inverse quantum Fourier transform,

$$\mathbf{H}_d^\dagger = \frac{1}{\sqrt{d}} \sum_{n,\ell'=0}^{d-1} e^{-i\frac{2\pi}{d}n\ell'} |n\rangle\langle\ell'|. \quad (15)$$

The resulting joint state is therefore

$$\begin{aligned} |\Psi_4\rangle &= \left(\mathbf{H}_d^\dagger \otimes \mathbb{1}_{d'}^{\otimes N} \right) |\Psi_3\rangle \\ &= \frac{1}{d} \sum_{n,\ell=0}^{d-1} \sum_x c_x e^{-i(\omega_x t + \frac{2\pi}{d}n)\ell} |n\rangle \otimes |x\rangle. \end{aligned} \quad (16)$$

Finally, the algorithm terminates by measuring the ancilla qudit. Before discussing this measurement step, we examine the projections of the final joint quantum state.

4. Final state projections

Projecting the final joint state $|\Psi_4\rangle$ onto $|n\rangle \otimes |\psi\rangle$ yields the amplitude

$$\begin{aligned} A(n) &= \langle n| \otimes \langle \psi| |\Psi_4\rangle \\ &= \frac{1}{d} \sum_{\ell=0}^{d-1} \sum_x |c_x|^2 e^{-i(\omega_x t + \frac{2\pi n}{d})\ell}. \end{aligned} \quad (17)$$

The sum in ℓ can be recognized as a discrete Fourier transform, which leads to the Dirichlet kernel[23], as demonstrated in Appendix A, then

$$A(n) = \frac{e^{i\pi n}}{d} \sum_x |c_x|^2 e^{-i\omega'_x \frac{t}{2}} \frac{\sin\left(\omega_x \frac{td}{2}\right)}{\sin\left(\omega_x \frac{t}{2} + \frac{\pi n}{d}\right)}. \quad (18)$$

where $\omega'_x = (d-1)\omega_x$. The corresponding probability distribution for measuring the ancilla qudit in the n -th level is therefore

$$\begin{aligned} P_d(n) &= |A(n)|^2, \\ &= \frac{1}{d^2} \left| \sum_x |c_x|^2 e^{-i\omega'_x \frac{t}{2}} \frac{\sin\left(\omega_x \frac{td}{2}\right)}{\sin\left(\omega_x \frac{t}{2} + \frac{\pi n}{d}\right)} \right|^2. \end{aligned} \quad (19)$$

Normalization follows directly from the orthogonality of the discrete Fourier basis.

5. Specific cases

In its original formulation, the Rodeo algorithm requires a hypothesized solution to the eigenvalue problem as input. A key requirement of this approach, as emphasized by the original authors, is that the input state exhibits substantial overlap with the target eigenstate of the Hamiltonian. Several strategies are proposed for constructing such an initial state, including preparation guided by physical intuition regarding the structure of the system's wave functions [11].

In the idealized case where the input state closely approximates an eigenstate, $|\psi\rangle \simeq |x\rangle$, the overlap coefficients satisfy $|c_{x'}|^2 \approx \delta(x-x')$. Under this assumption, the probability distribution for the ancilla measurement outcome simplifies to

$$P_d(n) \approx \frac{1}{d^2} \left| \frac{\sin\left(\omega_x \frac{td}{2}\right)}{\sin\left(\omega_x \frac{t}{2} + \frac{\pi n}{d}\right)} \right|^2. \quad (20)$$

Successful solution of the eigenproblem corresponds to measuring the ancilla in the state $|n\rangle = |0\rangle$. The associated success probability is therefore

$$P_d(0) \approx \frac{1}{d^2} \left| \frac{\sin\left(\omega_x \frac{td}{2}\right)}{\sin\left(\omega_x \frac{t}{2}\right)} \right|^2. \quad (21)$$

In the qubit case, corresponding to $d = 2$, this expression reduces to

$$P_2(0) \approx \cos^2 \left[(E_x - E) \frac{t}{2} \right], \quad (22)$$

where we have used the trigonometric identity $\sin(2\theta) = 2 \cos(\theta) \sin(\theta)$. This result is in direct agreement with the success probability obtained in the original formulation of the Rodeo algorithm.

The behavior of eqn (20) is illustrated in FIG. 2. Panel (a) displays the success probability for different ancilla dimensions: the qubit case ($d = 2$) is represented by the solid black curve, the qutrit ($d = 3$) by the dashed blue curve, and the ququart ($d = 4$) by the dash-dotted green curve. Panel (b) shows the probability distribution for measuring the ancilla qutrit in its different levels. The probability of observing the state $n = 0$ is shown by the solid black curve, $n = 1$ by the dashed blue curve, and $n = 2$ by the dash-dotted green curve. The dotted red curve corresponds to the sum over all values of n , demonstrating the normalization of the probability distribution.

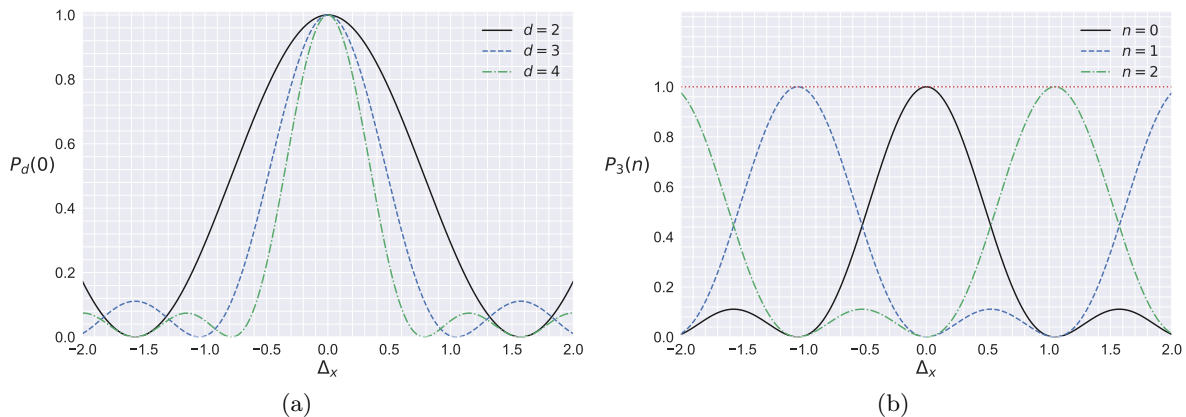


FIG. 2. (Color online) Probability of measuring a d -level ancilla qudit in the n th state when the system is prepared in a Hamiltonian eigenstate [see eqn. (20)], where here $\Delta_x = \omega_x t d / 2$. (a) Probability distribution for $n = 0$ and $d = 2, 3$, and 4. (b) Probability distribution for $d = 3$ and $n = 0, 1$, and 2; the dotted red curve corresponds to the sum over all n .

Owing to the large diversity of possible states, the width of the success-probability distribution becomes progressively narrower as the qudit dimension increases. On the other hand, the expectation values are likely to be less affected, since they correspond to a sum over the probabilities of all states, as discussed further.

B. Statistical Procedures

Within the Copenhagen interpretation of quantum mechanics, physical observables are not assigned definite values prior to measurement; rather, only probabilistic measurement outcomes are meaningful. Accordingly, the relevant quantities to analyze in the Rodeo algorithm are its measurement statistics.

1. Z_d expectation value

The measurement is implemented by projecting the final quantum state onto the observable Z_d , commonly referred to as the *clock operator*, whose eigenbasis defines the computational measurement basis. By definition [22],

$$Z_d = \sum_{n=0}^{d-1} \omega^n |n\rangle \langle n| = \sum_{n=0}^{d-1} e^{i \frac{2\pi n}{d}} |n\rangle \langle n|. \quad (23)$$

The clock operator can equivalently be expressed as

$$Z_d = \mathbf{H}_d^\dagger X_d \mathbf{H}_d, \quad (24)$$

where

$$X_d = \sum_{\ell=0}^{d-1} |(\ell+1) \bmod d\rangle \langle \ell|, \quad (25)$$

denotes the shift operator, satisfying $X_d |n\rangle = |n+1\rangle$. The modular operation ensures that $X_d |d-1\rangle = |0\rangle$, thereby imposing periodic boundary conditions on the finite-dimensional computational basis. This condition is important for further discussion.

We interpret the measurement outcome as the ancilla qudit level, $n = 0, 1, \dots, d-1$, thereby enabling direct determination of the coefficients of the Z_d operator. Thus, we are effectively measuring the clock operator eigenvalues. The corresponding measurement signal is defined as the expectation value

$$h_d(E, \psi | t) = \langle Z_d \otimes \mathbf{1}_{d'}^{\otimes N} \rangle = \langle \Psi_4 | (Z_d \otimes \mathbf{1}_{d'}^{\otimes N}) | \Psi_4 \rangle, \quad (26)$$

which explicitly evaluates to

$$h_d(E, \psi | t) = \frac{1}{d^2} \sum_{\ell, p, n=0}^{d-1} \sum_x |c_x|^2 e^{-i[\omega_x t(\ell-p) + \frac{2\pi n}{d}(\ell-p-1)]}. \quad (27)$$

The sum over n is identified as the discrete Fourier transform over the finite cyclic group of order d , yielding

$$\sum_{n=0}^{d-1} e^{-i\frac{2\pi n}{d}(\ell-p-1)} = d \delta_{\ell, s}, \quad (28)$$

where $s = (p+1) \bmod d$, then eqn. (27), can be written as

$$h_d(E, \psi | t) = \frac{1}{d} \sum_{\ell, p=0}^{d-1} \sum_x |c_x|^2 e^{-i[\omega_x t(\ell-p)]} \delta_{\ell, s}. \quad (29)$$

The Kronecker delta, $\delta_{\ell, s}$, constrains the index pairs (ℓ, p) to satisfy $\ell = (p+1) \bmod d$. Thus, for $p = 0, 1, \dots, d-2$, the only surviving contributions arise from index pairs satisfying $\ell - p = 1$. There are $(d-1)$ such pairs, each contributing a term proportional to $e^{-i\omega_x t}$. The remaining contribution originates from the periodic boundary condition of the finite-dimensional basis, corresponding to the pair $p = d-1$ and $\ell = 0$. In this case, $\ell - p = -(d-1)$, which yields a term proportional to $e^{+i(d-1)\omega_x t}$. Collecting all d contributions, we can define the Rodeo Kernel as

$$K_d(\omega_x, t) = \frac{d-1}{d} e^{-i\omega_x t} + \frac{1}{d} e^{+i\omega'_x t}, \quad (30)$$

recalling that $\omega'_x = (d-1)\omega_x$. Therefore, the expectation value takes the exact form

$$h_d(E, \psi | t) = \sum_x |c_x|^2 K_d(\omega_x, t). \quad (31)$$

It is worth noting that, if the input system state is an eigenstate of the Hamiltonian, $|\psi\rangle = |x\rangle$, just one coefficient survives in eqn. (31), then $h_d(E, x | t) = K_d(\omega_x, t)$. Moreover, the Rodeo Kernel can be seen as a two-frequency interferometer: a high-amplitude, low-frequency signal and a low-amplitude, high-frequency signal. The dependence of the expectation value on the ancilla dimension arises from interference between the two signals. In the ancilla qubit implementation, $d = 2$, these two terms combine to give

$$h_2(E, \psi | t) = \sum_x |c_x|^2 \cos[(E_x - E)t], \quad (32)$$

in agreement with the existing literature [13, 24]. In this situation, the signal contains a single-frequency component; therefore, no interference occurs. Consequently, interference effects first appear in qutrit implementation ($d = 3$). Moreover, for $d = 3$, the higher-frequency term lies closer to resonance and has a larger

amplitude than for $d > 3$. So the interplay between the two frequency components is expected to be most pronounced in the qutrit implementation.

Alternatively, in terms of the Loschmidt amplitude

$$L(t) = \sum_x |c_x|^2 e^{-i(E_x - E)t}, \quad (33)$$

eqn. (31) can be expressed as

$$h_d(E, \psi | t) = \frac{d-1}{d} L(t) + \frac{1}{d} L^*(t)^{d-1}, \quad (34)$$

where $L^*(t)$ denotes the complex conjugate of the Loschmidt amplitude. The second term constitutes a harmonic contamination of weight $1/d$ that vanishes in the limit $d \rightarrow \infty$, recovering $h \rightarrow L(t)$ exactly, thereby corroborating the interpretation of the Rodeo algorithm as a realization of a Loschmidt echo [25].

2. Ensemble average

We define the *spectral amplitude* (SA) of the Rodeo algorithm as the ensemble average of the expectation value of the operator $Z_d \otimes \mathbb{1}^{\otimes N}$. It is the mean value of $h_d(E, \psi | t)$ over repeated realizations of the algorithm, where the evolution time t is randomly sampled from a probability density function (PDF) denoted by $P(t | \{X\})$. Here, $\{X\}$ represents the set of parameters characterizing the PDF. The SA is therefore quantified by

$$G_d(E, \psi) = \int_{-\infty}^{\infty} h_d(E, \psi | t) P(t | \{X\}) dt. \quad (35)$$

Following the original formulation of the Rodeo algorithm, we choose the PDF to be a normal (Gaussian) distribution,

$$P(t | \mu, \sigma) = \frac{1}{\sigma\sqrt{2\pi}} e^{-\frac{(t-\mu)^2}{2\sigma^2}}, \quad (36)$$

where the set of parameters $\{X\} = \{\mu, \sigma\}$, denote the mean and standard deviation, respectively. The Gaussian distribution is relevant for specific interpretations of the algorithm considered in this work. Substituting eqn. (36) and (31) into eqn. (35) yields

$$G_d(E, \psi) = \sum_x |c_x|^2 (TP)(\omega_x) \quad (37)$$

where

$$(TP)(\omega_x) = \frac{d-1}{d} \left(\frac{1}{\sigma\sqrt{2\pi}} \int_{-\infty}^{\infty} e^{-\frac{(t-\mu)^2}{2\sigma^2}} e^{-i\omega_x t} dt \right) + \frac{1}{d} \left(\frac{1}{\sigma\sqrt{2\pi}} \int_{-\infty}^{\infty} e^{-\frac{(t-\mu)^2}{2\sigma^2}} e^{i\omega'_x t} dt \right). \quad (38)$$

We adopt the general notation for the integral transform. Particularly, these integrals can correspond to the Fourier transform of a Gaussian and can be computed analytically:

$$\frac{1}{\sigma\sqrt{2\pi}} \int_{-\infty}^{\infty} e^{\pm i\omega t} e^{-\frac{(t-\mu)^2}{2\sigma^2}} dt = e^{-\frac{\sigma^2\omega^2}{2}} e^{\pm i\omega\mu}, \quad (39)$$

Then leading to

$$(TP)(\omega_x) = \frac{d-1}{d} e^{-\frac{\sigma^2\omega_x^2}{2}} e^{-i\omega_x\mu} + \frac{1}{d} e^{-\frac{\sigma^2\omega'_x{}^2}{2}} e^{+i\omega'_x\mu}. \quad (40)$$

In our numerical evaluation, we set $\mu = 0$ to eliminate the oscillatory phase factor and focus exclusively on the spectral filtering properties of the SA. In this case, the expression simplifies to

$$\begin{aligned} (TP)(\omega_x) &= \frac{d-1}{d} e^{-\frac{\sigma^2\omega_x^2}{2}} + \frac{1}{d} e^{-\frac{\sigma^2\omega'_x{}^2}{2}}, \\ &= e^{-\frac{\sigma^2\omega_x^2}{2}} \left[1 - \left(\frac{1 - e^{-\frac{\sigma^2(\omega'_x{}^2 - \omega_x^2)}{2}}}{d} \right) \right]. \end{aligned} \quad (41)$$

For finite ω_x , the Gaussian damping in the second term is much stronger than that of the main term. Thus, the higher-frequency harmonic contamination decays rapidly, underscoring its perturbative nature. For $d = 2$, $\omega'_x = \omega_x$, so the perturbative term is canceled out, leading to

$$G_2(E, \psi) = \sum_x |c_x|^2 e^{-\frac{\sigma^2(E_x - E)^2}{2}}, \quad (42)$$

corroborating our previous result [13, 24], where we interpreted the SA as the probability to measure the system state $|\psi\rangle$ with a given energy E . Moreover, the limit $d \rightarrow \infty$ of eqn. (41) recovers the result for the ancilla qubit implementation. These results therefore support the conjecture that the expectation values are only weakly affected by the ancilla qudit's dimension.

To create a metric for the perturbative effects, let us define the relative difference between the SA obtained using an ancilla qudit and that obtained with an ancilla qubit as

$$\Delta_2 G_d(E, \psi) = 1 - \frac{G_d(E, \psi)}{G_2(E, \psi)}. \quad (43)$$

Since the Gaussian dumping in $G_d(E, \psi)$ is stronger than in $G_2(E, \psi)$ —that is, the former approaches zero faster than the latter—this relation can be considered well defined over the entire energy range.

We aim to show that the Rodeo algorithm can be adapted into a quantum protocol for estimating the density of states (DoS), from which thermodynamic quantities such as the microcanonical entropy can be obtained directly.

C. Single-state microcanonical protocol

Recently, we proposed a protocol based on the Rodeo algorithm for estimating the entropy of a quantum system [24]. The protocol consists of summing the SA over all computational basis states used to represent the system. A central limitation of this protocol is the exponential growth of the Hilbert-space dimension: for an N -particle system composed of d' -level subsystems, the computational basis contains d'^N states. To mitigate this issue, we consider preparing the input state as a homogeneous superposition of the Hamiltonian eigenstates,

$$|\psi_{\{x\}}\rangle = \frac{1}{\sqrt{d'^N}} \sum_x |x\rangle, \quad (44)$$

for which the overlap coefficients satisfy $|c_x|^2 = 1/d'^N$. Since the SA can be interpreted as the probability of finding the input state ψ at energy E , and the homogeneous input state has equal overlap with all energy eigenstates, with degeneracies properly accounted, the SA effectively reconstructs the density of states (DoS) at energy E . Mathematically, considering the limit

$$\lim_{\sigma \rightarrow \infty} G_d(E, \psi) = \sum_x |c_x|^2 \delta(E_x - E), \quad (45)$$

and substituting eqn. (44) into eqn. (37), together with eqn. (41), yields

$$\begin{aligned} G_d(E, \psi_{\{x\}}) &:= g_d(E) \\ &\approx \frac{1}{d'^N} \sum_x \delta(E_x - E) = \frac{\Omega(E)}{d'^N}. \end{aligned} \quad (46)$$

This approach directly connects the SA with the DoS. The microcanonical entropy,

$$S(E) = k_B \ln g(E) + C, \quad (47)$$

where k_B is the Boltzmann constant and $C = Nk_B \ln d'$, then follows naturally[26]. This formulation therefore provides a framework for studying quantum effects in thermodynamic systems [27].

It is instructive to build an analogy with the canonical partition function. The eqn. (42) for the homogeneous input can be written as

$$\begin{aligned} G_2(E, \psi_{\{x\}}) &= \frac{1}{d^N} \sum_x e^{-\frac{\sigma^2(E_x - E)^2}{2}}, \\ &= \frac{1}{d^N} \text{Tr} \left[e^{-\frac{\sigma^2}{2}(\mathcal{H} - E\mathbf{1})^2} \right]. \end{aligned} \quad (48)$$

On the other hand, the canonical partition function is given by

$$\begin{aligned} Z(\beta) &= \text{Tr} (e^{-\beta\mathcal{H}}), \\ &= \int \Omega(E) e^{-\beta E} dE, \end{aligned} \quad (49)$$

Then, by analogy, we may write

$$\begin{aligned} \text{Tr} \left[e^{-\frac{\sigma^2}{2}(\mathcal{H} - E\mathbf{1})^2} \right] &= \int \Omega(E') e^{-\frac{\sigma^2}{2}(E' - E)^2} dE', \\ &= (\Omega * P')(E), \end{aligned} \quad (50)$$

where $P'(E' - E) = \exp[-\sigma^2(E' - E)^2/2]$ is the Fourier transform of the Gaussian distribution. Since the Fourier transform of a Fourier series is a set of impulses, as $\Omega(E) = \sum_x \delta(E_x - E)$, then eqn. (42) follows directly from the convolution theorem,

$$(u * v) = \mathcal{F}\{\mathcal{F}^\dagger\{u\}\mathcal{F}^\dagger\{v\}\}, \quad (51)$$

corroborating with the analogy. Moreover, the convolution recovers $\Omega(E)$ in a smoothed form, $\Omega_\sigma(E)$, whose width is determined by σ . Consequently, the approach in eqn. (46) becomes the identity

$$g_d(E) = \frac{\Omega_\sigma(E)}{d^N}, \quad (52)$$

when $g_d(E)$ is interpreted as the smoothed density of states. This convolution structure reveals that the Rodeo algorithm acts as a spectral filter that applies Gaussian smoothing to the Hamiltonian spectrum.

This formulation, therefore, realizes a microcanonical ensemble protocol [28, 29], in which the DoS is estimated from a single input state given by eqn. (44). Although the protocol avoids explicit enumeration of the exponentially large computational basis, it remains statistically limited: Small $g(E)$ values become difficult to distinguish from statistical fluctuations, as further discussed.

III. NUMERICAL EVALUATION

In this section, we present a numerical analysis of the Rodeo algorithm based on a numerical linear-algebra evaluation of the joint ancilla-system state as it evolves through the Rodeo circuit. We apply the method to the one-dimensional Lenz-Ising model, described by the Hamiltonian

$$\mathcal{H}_{d'} = -J \sum_{\langle i, j \rangle} \mathbf{1}_{d'}^{\otimes i} \otimes S_{d', i}^z \otimes S_{d', j}^z \otimes \mathbf{1}_{d'}^{\otimes (N-1-j)} \equiv -J \sum_{\langle i, j \rangle} S_i^z S_j^z, \quad (53)$$

where the symbol $\langle i, j \rangle$ denotes the indices satisfy $i = 0, \dots, N-1$ and $j = i+1$, where N is the number of particles in the chain. Periodic boundary conditions are assumed, so that site N is identified with site 0. The factor $\mathbf{1}^{\otimes 0}$ is understood as the absence of this identity operator in the tensor product. The parameter J is the exchange coupling constant, and $S_{d', i}^z$ is the spin operator along the z direction acting on the i -th particle in a d' -dimensional Hilbert space. In our choice of units, energy is measured in units of JS^2 , where S denotes the spin magnitude.

In the graphs presented here, black dots denote the numerical evaluations, and error bars represent the associated standard deviations. Solid red curves represent theoretical predictions, and vertical blue lines, when present, indicate exact values.

A. 1D Spin $1/2$ Ising Model

In FIG. 3 we present the results for the regular one-dimensional spin- $1/2$ Ising model. For this case ($d' = 2$), S_2^z corresponds to the Pauli- Z matrix,

$$S_2^z = \begin{pmatrix} 1 & 0 \\ 0 & -1 \end{pmatrix} = |0\rangle\langle 0| - |1\rangle\langle 1|. \quad (54)$$

We consider a chain of $N = 5$ particles. The evolution times are sampled from a Gaussian distribution with $\sigma = 5$. The theoretical prediction is given by eqn (41). Panels (a) and (b) use the initial state

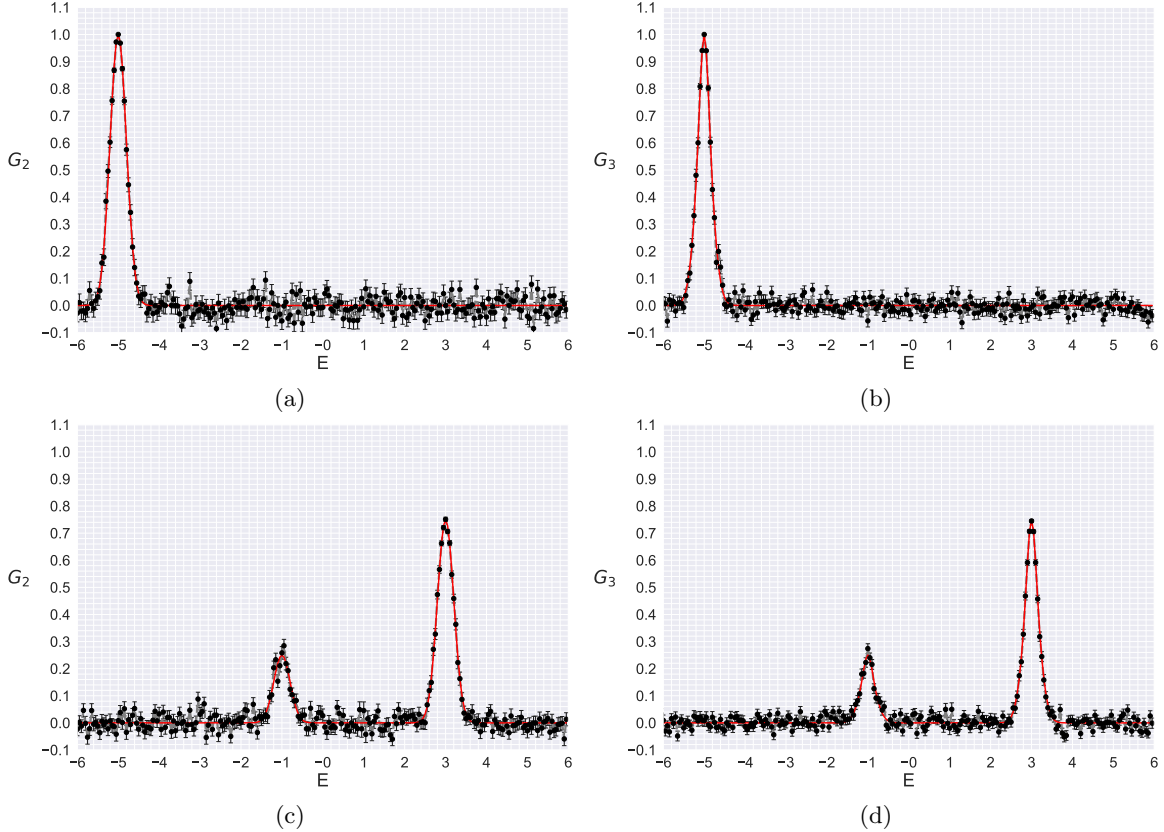


FIG. 3. (Color online) Numerical evaluation of the Rodeo algorithm applied to the one-dimensional spin- $1/2$ Ising model with $N = 5$ spins. The averages are over 500 distinct evolution times per energy level, drawn from a Gaussian distribution with $\sigma = 5$. Panels (a) and (b) for system state $|\psi\rangle = |0\rangle$, while panels (c) and (d) $|\psi\rangle = 1/2|1\rangle + \sqrt{3}/2|5\rangle$. In panels (a) and (c), the ancilla qubit ($d = 2$) implementation, and (b) and (d) the ancilla qutrit ($d = 3$) is employed. The local maxima of \bar{h} are interpreted as the probabilities of measuring the state $|\psi\rangle$ at energy E .

$|\psi\rangle = |0\rangle$, which is a system eigenstate with energy $E_0 = -5$. Panels (c) and (d) consider the superposition $|\psi\rangle = 1/2|1\rangle + \sqrt{3}/2|5\rangle$, which is a linear combination of the eigenstate $|1\rangle$ with eigenvalue $E_1 = -3$, and the eigenstate $|5\rangle$ with eigenvalue $E_5 = 1$. The results empirically demonstrate that the local maxima of the SA correspond to the probability of measuring the input state at the peak energy. In panels (a) and (c), the controlled time evolution is implemented with an ancilla qubit ($d = 2$), whereas in panels (b) and (d) an ancilla qutrit ($d = 3$) is employed.

A visual inspection of the figure indicates that, when comparing the ancilla qutrit with the ancilla qubit, the spectral peak becomes narrower and the fluctuations are reduced for energy values away from the peak position. To quantify these effects, we introduce two metrics. First, we consider the relative difference between the SA obtained using an ancilla qutrit and that obtained with an ancilla qubit, which characterizes the narrowing of the peak. Second, in the region where the SA is approximately zero, the fluctuation is quantified by the standard deviation of the measured points.

We first analyze the peak narrowing. For an eigenstate input, $|\psi\rangle = |x\rangle$, eqn. (43), which governs the relative difference, can be written as

$$\Delta_2 G_d(E, x) = \frac{1 - e^{-\frac{\sigma^2(d^2 - 2d)(E_x - E)^2}{2}}}{d}. \quad (55)$$

This relation is constrained to the interval $0 \leq \Delta_2 G_d(E, x) \leq d^{-1}$, which implies $G_2(E, x) \geq G_d(E, x)$. This behavior is illustrated in FIG. 4 for $|x\rangle = |0\rangle$. Panel (a) shows a comparison for $d = 3, 4$, and 5 via directly plot of the eqn. (55). As discussed previously, the perturbation in the peak decay tends to zero as d increases. Panels (b), (c), and (d) demonstrate that the numerical results corroborate the theoretical prediction, for $d = 3, 4$, and 5 , respectively. Due to error propagation, which leads to error bars that are inversely proportional to \hbar_2 , we display only the peak-decay region. The implementation employing an ancilla qutrit shows the strongest peak narrowing.

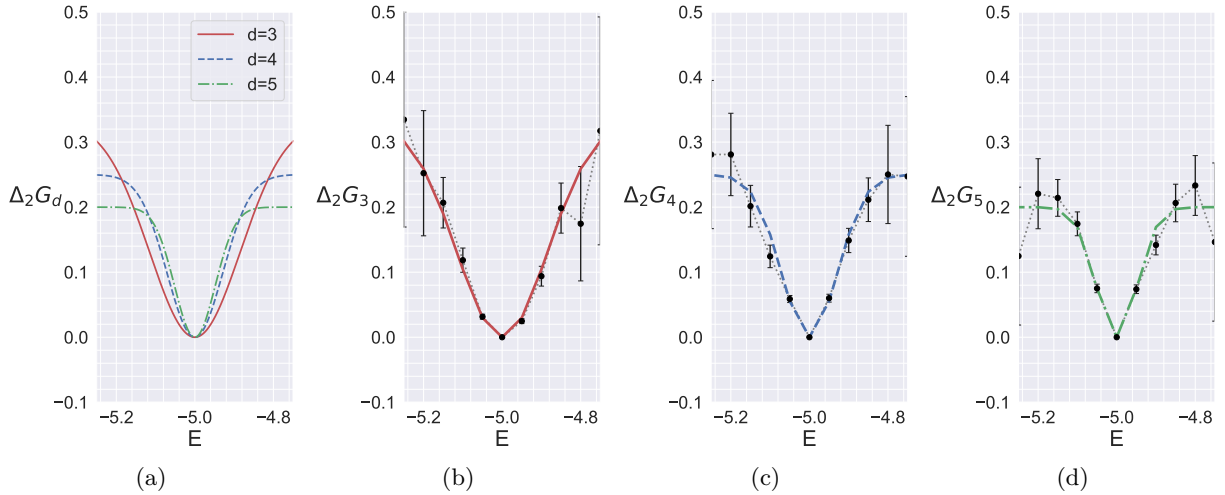


FIG. 4. Relative difference of the spectral amplitude obtained with a d -dimensional ancilla qudit with respect to the ancilla qubit case ($d = 2$) for the one-dimensional spin- $\frac{1}{2}$ Ising model with input state $|\psi\rangle = |0\rangle$. The Gaussian distribution used in the averaging has $\sigma = 5$. Panel (a) shows the theoretical prediction for different ancilla dimensions (see eqn (55)). Panels (b)–(d) display the corresponding numerical results for a periodic chain of five spins, obtained from 500 independent realizations of the evolution time for each energy value: (b) $d = 3$, (c) $d = 4$, and (d) $d = 5$.

Although the fluctuations are quantified by the standard deviation of the numerical data across different energy values, we conjecture that they are, to some extent, associated with the error bars. This is justified by the fact that all energy values in the region of interest are subject to the same statistical behavior. Since $h(E, \psi|t)$ is a complex quantity, the ensemble averages of its real and imaginary parts were computed separately in the numerical evaluations. In Appendix B 2 demonstrates that the maximum standard deviation for the specific case when the input state is equal to the energy eigenvalue, $|\psi\rangle = |x\rangle$, is given by

$$\text{std}_m[\text{Re}(h_d(E, x))] = \text{std}_m[\text{Im}(h_d(E, x))] = \frac{1}{d} \sqrt{\frac{d^2 - 2d + 2}{2N_t}}, \quad (56)$$

while the average of the imaginary part of $h(E, \psi|t)$ is zero. As discussed in this appendix, eqn. (56) does not apply for $d = 2$, since in this case the signal is purely real. For the ancilla qubit implementation, the maximum standard deviation is $\sqrt{2}$ times the value obtained by evaluating eqn. (56) at $d = 2$. Due to this $\sqrt{2}$ factor, the ancilla qubit implementation exhibits the largest standard deviation, equal to the limit $d \rightarrow \infty$. Moreover, the ancilla qutrit yields the smallest predicted value, corresponding to a theoretical reduction of up to 25% in dispersion compared to the qubit implementation.

In Table I, we compare the theoretical predictions with the numerical estimates. The first column indicates the ancilla qudit dimensionality. The second column corresponds to the direct evaluation of eqn (56), considering $N_t = 500$, which is the number of realizations used in our numerical simulations. The third column reports the average of the error bars in the region $G_d(E, x) < 0.1$ (the uncertainties were computed from five

independent simulations). We observe excellent agreement between the theoretical and numerical values. The fourth column shows the fluctuation metric, previously discussed. Finally, the last column presents the reduction ratio, defined as the relative difference between the numerical estimates of the fluctuations for the ancilla-qudit and ancilla-qubit implementations.

TABLE I. Comparison between theoretical predictions and numerical estimates of the standard deviations associated with the Rodeo algorithm. The first column shows the ancilla qudit dimension d . The second and fourth columns give the theoretical standard deviations from the analytical expressions. The third column reports the mean error bar, the fifth column reports the fluctuation of the numerical data along the energy axis, and the last column reports the relative difference between the fluctuation of the ancilla qudit and that of the ancilla qubit implementation.

d	std_{max}	Error bar	Fluctuation	reduction ratio
2	~ 0.03162	0.03164(1)	0.0338(2)	-
3	~ 0.02357	0.02354(1)	0.0276(3)	18.3%
4	0.025	0.02497(1)	0.0278(5)	17.8%
5	~ 0.02608	0.02600(1)	0.0292(1)	13.6%
∞	~ 0.03162	-	-	-

Although discrepancies between the theoretical prediction and the numerical estimates, ranging from 7% to 17%, are observed, we interpret the fluctuations of the data points across different energies as reflecting the standard deviation indicated by the error bars. As conjectured, the ancilla qutrit implementation provides enhanced noise reduction and improved spectral resolution, yielding an 18% reduction in fluctuations. Although smaller than the theoretically predicted 25%, this reduction remains significant.

B. 1D Spin-1 Ising Model

As an illustrative example of a multi-level quantum system, we consider the one-dimensional spin-1 Lenz-Ising model, for which the local Hilbert-space dimension is $d' = 3$. In this case, the spin operator along the z -direction can be written as

$$S_3^z = \begin{pmatrix} 1 & 0 & 0 \\ 0 & 0 & 0 \\ 0 & 0 & -1 \end{pmatrix} = |0\rangle\langle 0| - |2\rangle\langle 2|. \quad (57)$$

In FIG. 5 (a), we present the SA for a chain of three particles with the input state $|15\rangle$. The state labels are written in decimal (radix-10) notation, but they can be interpreted in terms of spin configurations by converting the index to balanced ternary notation. Because the particle positions are labeled from left to right, the ternary digits must be read in reverse order. Under this convention, the state $|15\rangle$ corresponds to the configuration $|0, -1, 1\rangle$, or in a pictorial z -component representation, $|\circ, \downarrow, \uparrow\rangle$. The corresponding energy eigenvalue is $E_{15} = +1$, which the SA accurately recovers. The results presented here were obtained by sampling 500 realizations of the evolution time from a normal distribution with standard deviation $\sigma = 10$.

FIG. 5 (b) shows the resulting number of states (NoS) for the system corresponding to the input state considered in panel (a). The NoS is obtained by summing the spectral amplitude (SA) over all computational basis states used to represent the system. The agreement between these results shows that the positions of the spectral peaks correctly reproduce the degeneracy density of the energy levels.

FIG. 6 shows the result for the single-input microcanonical protocol of the Rodeo algorithm for the one-dimensional spin-1 Ising model with $N = 5$ particles. Panels (a) and (b) correspond to the ancilla qubit and ancilla qutrit implementations, respectively. As expected, the qutrit implementation yields reduced noise and enhanced spectral resolution. The SA in this protocol is interpreted as the DoS, here computed from 3000 independent realizations of the evolution time for each energy value, sampled from a Gaussian distribution with $\sigma = 20$. The results clearly exhibit the Gaussian smoothing of the energy spectrum, confirming that the protocol effectively performs a Gaussian convolution of the spectral density.

This figure illustrates the compromise between computational cost and statistical precision. Although the qutrit implementation provides some degree of noise reduction, identifying the ground-state degeneracy

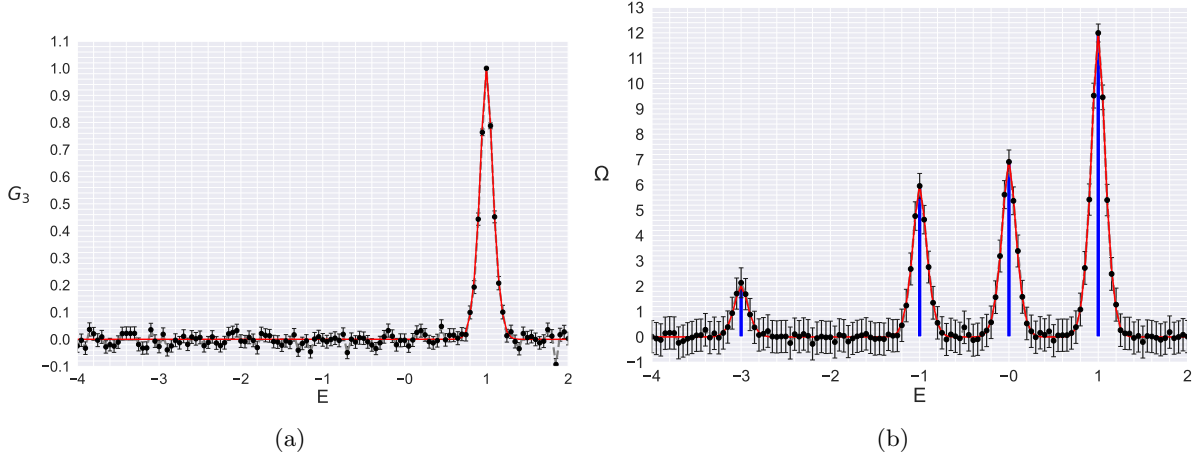


FIG. 5. Numerical evaluation of the Rodeo algorithm applied to the one-dimensional spin-1 Ising model with $N = 3$ spins. The evolution times are sampled from a Gaussian distribution with $\sigma = 10$. Panel (a) shows the SA for the input state $|\psi\rangle = |15\rangle$, where the averages are taken over 500 distinct evolution times for each energy value. Panel (b) presents the cumulative result obtained by summing the SA over all computational basis states, which reconstructs the degeneracy of the system.

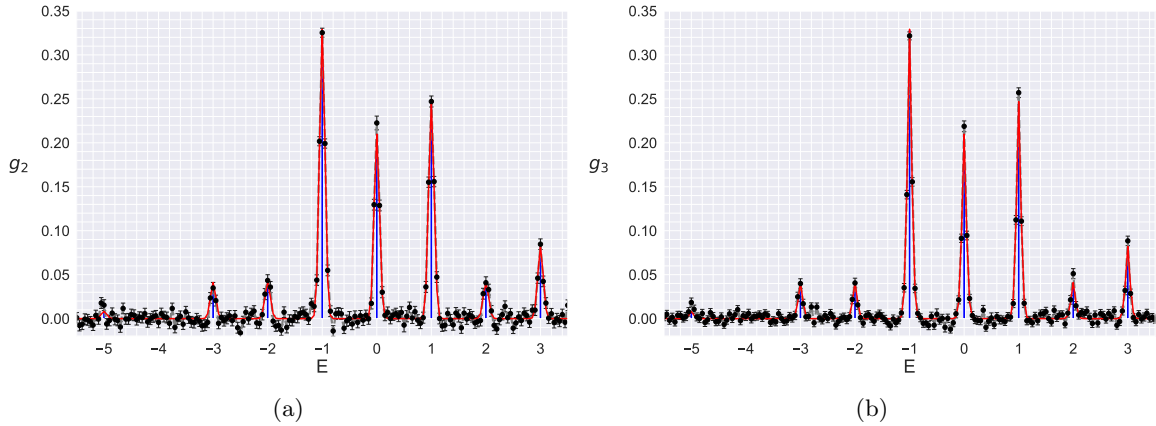


FIG. 6. Single-input microcanonical protocol for the Rodeo Algorithm applied to the one-dimensional Ising model. We consider a periodic chain of five spins. The black dots represent the average from 3000 independent realizations of the evolution time for each energy value, while the error bars denote the corresponding standard deviations. The evolution times are sampled from a Gaussian distribution with $\sigma = 20$. Panels (a) the controlled time evolution is implemented with an ancilla qubit ($d = 2$), while in panels (b) an ancilla qutrit ($d = 3$) is employed.

remains challenging for $N_t = 3000$, even when using an ancilla qutrit. Nevertheless, partial knowledge of the density of states (DoS) is often sufficient to describe the thermodynamic behavior of a physical system, particularly when the analysis focuses on a narrow region of the thermodynamic coordinate space.

IV. CONCLUSION

In this work, we developed a qudit formulation of the Rodeo algorithm and analyzed its theoretical and numerical properties. By deriving the full quantum-circuit evolution for a general d -level ancilla, we showed that the width of the success-probability distribution becomes progressively narrower as the qudit dimension increases. Nevertheless, the effects on the expectation values appear only as perturbative corrections, which first arise in the qutrit implementation and diminish as d increases.

These perturbative effects are particularly relevant for noise reduction and spectral resolution enhance-

ment. We demonstrated that the periodic boundary conditions imposed by the finite-dimensional computational basis give rise to a two-frequency interference structure for $d > 2$. This interference divides the variance of the quantum expectation value between real and imaginary components, leading to a $1/\sqrt{2}$ reduction of the noise in the ensemble average over repeated executions of the algorithm. Moreover, the higher-frequency contribution is more strongly damped by the average Gaussian, whereas its amplitude decreases with increasing d . Consequently, the effect is most pronounced for the qutrit implementation, since the interfering frequency components exhibit smaller differences in both frequency and amplitude compared with higher-dimensional cases.

We also introduced a single-state microcanonical protocol for the Rodeo algorithm. This protocol yields a Gaussian-smoothed density of states for the quantum system by effectively implementing a Gaussian convolution of the energy spectrum. Consequently, the entropy can be estimated from a single energy sweep of the Rodeo algorithm. However, a trade-off arises between computational effort and statistical precision.

As a perspective, we intend to study other statistical distributions for the evolution time, aiming to characterize the smoothing behavior in the convolution associated with the microcanonical protocol.

Finally, our results highlight that multi-level qudits provide a natural and efficient framework for investigating quantum systems with multi-level degrees of freedom and may offer new opportunities for quantum spectral analysis and thermodynamic characterization of many-body systems.

AUTHOR DECLARATIONS

This research received no specific grant from any funding agency in the public, commercial, or not-for-profit sectors.

The authors used large language models (Claude Anthropic and OpenAI ChatGPT) to improve the grammar and clarity of this manuscript. The AI was prompted to review flow and conciseness, but all content, interpretations, and conclusions were verified and edited by the authors, who take full responsibility for the integrity of the work.

Conflict of Interest Statement

The authors have no conflicts to disclose.

Author Contributions

Julio C.S. Rocha leads conceptualization, methodology, writing original draft, software, data curation, formal analysis, and visualization.

Rodrigo A. Dias supporting conceptualization, data curation, visualization, and software.

DATA AVAILABILITY STATEMENT

The data that support the findings of this study is openly available in reference number ? .

Appendix A: Projection Amplitude

To prove eqn. (18), we define

$$\theta_x(n) = 2\omega_x t + \frac{2\pi n}{d}. \quad (\text{A1})$$

Using the finite geometric series identity

$$\sum_{\ell=0}^{d-1} e^{-i\ell\theta} = \frac{1 - e^{-i\theta d}}{1 - e^{-i\theta}} = e^{-i\frac{(d-1)\theta}{2}} \frac{\sin(\theta d/2)}{\sin(\theta/2)}, \quad (\text{A2})$$

where $\sin \theta = (e^{i\theta} - e^{-i\theta})/(2i)$, the above expression can be recognized as the Dirichlet kernel [23] for non-negative integer ℓ .

The projection amplitude, eqn. (17), can then be written as

$$A(n) = \frac{1}{d} \sum_x |c_x|^2 e^{-i \frac{(d-1)\theta_x(n)}{2}} \frac{\sin(\theta_x(n)d/2)}{\sin(\theta_x(n)/2)}. \quad (\text{A3})$$

Substituting the definition of $\theta_x(n)$ into the numerator gives

$$\sin(\omega_x t d + \pi n) = e^{i\pi n} \sin(\omega_x t d), \quad (\text{A4})$$

which leads to eqn. (18):

$$A(n) = \frac{e^{i\pi n}}{d} \sum_x |c_x|^2 e^{-i\omega'_x t} \frac{\sin(\omega_x t d)}{\sin(\omega_x t + \pi n/d)}, \quad (\text{A5})$$

where $\omega'_x = (d-1)\omega_x$.

Appendix B: Calculation of variance and standard deviation

1. Variance of the expectation value

In this section, we analyze the variance of the spectral amplitude. By definition, the variance is

$$\text{Var}[h(E, \psi)] \equiv \overline{h^2(E, \psi)} - \left[\overline{h(E, \psi)} \right]^2, \quad (\text{B1})$$

where the overline denotes averaging with respect to the Gaussian time-sampling distribution introduced in Sec. II B 2.

2. Real part

The real part of eqn. (31) satisfies

$$\text{Re}(K_d(\omega_x, t)) = \frac{d-1}{d} \cos(\omega_x t) + \frac{1}{d} \cos(\omega'_x t). \quad (\text{B2})$$

Using

$$\frac{1}{\sigma\sqrt{2\pi}} \int_{-\infty}^{\infty} \cos(\omega t) e^{-\frac{(t-\mu)^2}{2\sigma^2}} dt = e^{-\frac{\sigma^2\omega^2}{2}} \cos(\omega\mu), \quad (\text{B3})$$

the Gaussian average of eqn. (B2) for $\mu = 0$ reduces to eqn. (41). Consequently, squaring this equation yields

$$\left[\overline{h_d(E, \psi)} \right]^2 = G^2(E, \psi) = \sum_{x,y} |c_x|^2 |c_y|^2 [(TP)(\omega_x)] [(TP)(\omega_y)],$$

where

$$[(TP)(\omega_x)] [(TP)(\omega_y)] = e^{-\frac{\sigma^2(\omega_x^2 + \omega_y^2)}{2}} \left[1 - \left(\frac{1 - e^{-\frac{\sigma^2(\omega_x'^2 - \omega_x^2)}{2}}}{d} \right) \right] \left[1 - \left(\frac{1 - e^{-\frac{\sigma^2(\omega_y'^2 - \omega_y^2)}{2}}}{d} \right) \right]. \quad (\text{B4})$$

For $|\psi\rangle = |x\rangle$ this relation becomes

$$\left[\overline{h_d(E, x)} \right]^2 = G^2(E, x) = [(TP)(\omega_x)]^2 = e^{-\sigma^2\omega_x^2} \left[1 - \left(\frac{1 - e^{-\frac{\sigma^2(\omega_x'^2 - \omega_x^2)}{2}}}{d} \right) \right]^2. \quad (\text{B5})$$

On the other hand, squaring eqn. (B2) gives

$$\begin{aligned} [\text{Re}(K_d(\omega_x, t))] [\text{Re}(K_d(\omega_y, t))] &= \frac{1}{d^2} \left\{ (d-1)^2 \cos(\omega_x t) \cos(\omega_y t) + \cos(\omega'_x t) \cos(\omega'_y t) \right. \\ &\quad \left. + (d-1) \left[\cos(\omega_x t) \cos(\omega'_y t) + \cos(\omega_y t) \cos(\omega'_x t) \right] \right\}. \end{aligned} \quad (\text{B6})$$

Using the identity $\cos a \cos b = [\cos(a-b) + \cos(a+b)]/2$ and considering $|\psi\rangle = |x\rangle$, we obtain

$$[\text{Re}(K_d(\omega_x, t))]^2 = \frac{1}{d^2} \left[(d-1)^2 \frac{1 + \cos(2\omega_x t)}{2} + \frac{1 + \cos(2\omega'_x t)}{2} \right] \quad (\text{B7})$$

$$+ (d-1) \left(\cos[(\omega'_x - \omega_x)t] + \cos[(\omega'_x + \omega_x)t] \right). \quad (\text{B8})$$

Performing the Gaussian average with $\mu = 0$ gives

$$\begin{aligned} ([\text{Re}(K_d)]^2 P)(\omega_x) &= \frac{1}{d^2} \left[(d-1)^2 \frac{1 + e^{-2\sigma^2 \omega_x^2}}{2} + \frac{1 + e^{-2\sigma^2 \omega_x'^2}}{2} \right. \\ &\quad \left. + (d-1) \left(e^{-\frac{\sigma^2}{2}(\omega'_x - \omega_x)^2} + e^{-\frac{\sigma^2}{2}(\omega'_x + \omega_x)^2} \right) \right]. \end{aligned} \quad (\text{B9})$$

Therefore, subtracting eqn. (B5) from the relation above leads to

$$\text{Var}[\text{Re}(h_d(E, x))] = \frac{1}{d^2} \left[(d-1)^2 \frac{1 + e^{-2\sigma^2 \omega_x^2}}{2} + \frac{1 + e^{-2\sigma^2 \omega_x'^2}}{2} \right] \quad (\text{B10})$$

$$+ (d-1) \left(e^{-\frac{\sigma^2}{2}(\omega'_x - \omega_x)^2} + e^{-\frac{\sigma^2}{2}(\omega'_x + \omega_x)^2} \right) \quad (\text{B11})$$

$$- e^{-\sigma^2 \omega_x^2} \left[1 - \left(\frac{1 - e^{-\frac{\sigma^2(\omega_x'^2 - \omega_x^2)}{2}}}{d} \right) \right]^2 \quad (\text{B12})$$

For $E = E_x$, i.e. $\omega_x = \omega'_x = 0$, it leads to $\text{Var}[\text{Re}(h_d(E_x, x))] = 0$. For energy values far away from the peak position, i.e., $\omega_x \gg 1$ (considering $d > 2$) we can identify the maximal variance as

$$\text{Var}_m[\text{Re}(h_d(E, x))] = \frac{(d-1)^2 + 1}{2d^2}. \quad (\text{B13})$$

For $d = 2$, one must recall that $\omega'_x = \omega_x$, so an additional term $(d-1)/d^2$ must be included in the relation above. Therefore

$$\text{Var}_m[\text{Re}(h_2(E, x))] = 0.5.$$

The maximal standard deviation for $d > 2$ is then:

$$\text{std}_m[\text{Re}(h_d(E, x))] = \frac{1}{d} \sqrt{\frac{d^2 - 2d + 2}{2N_t}}. \quad (\text{B14})$$

where N_t is the number of realizations of the evolution time. Since the standard deviation at the peak position is zero, this suggests an adaptive sampling strategy in which the number of algorithmic cycles is reduced in regions where the variance approaches its maximum.

3. Imaginary part

The imaginary part of eqn. (31) satisfies

$$\text{Im}(K_d(\omega_x, t)) = \frac{d-1}{d} \sin(\omega_x t) + \frac{1}{d} \sin(\omega'_x t). \quad (\text{B15})$$

For $\mu = 0$, the Gaussian average

$$\frac{1}{\sigma\sqrt{2\pi}} \int_{-\infty}^{\infty} \sin(\omega t) e^{-\frac{t^2}{2\sigma^2}} dt = 0 \quad (\text{B16})$$

vanishes because the integrand is an odd function.

Squaring eqn. (B15) yields

$$\begin{aligned} [\text{Im}(K_d(\omega_x, t))]^2 &= \frac{1}{d^2} \left\{ (d-1)^2 \sin(\omega_x t) \sin(\omega_y t) + \sin(\omega'_x t) \sin(\omega'_y t) \right. \\ &\quad \left. + (d-1) [\sin(\omega_x t) \sin(\omega'_y t) + \sin(\omega_y t) \sin(\omega'_x t)] \right\}. \end{aligned} \quad (\text{B17})$$

Using $\sin a \sin b = [\cos(a-b) - \cos(a+b)]/2$ and again taking $|\psi\rangle = |x\rangle$, we obtain

$$[\text{Im}(K_d(\omega_x, t))]^2 = \frac{1}{d^2} \left[(d-1)^2 \frac{1 - \cos(2\omega_x t)}{2} + \frac{1 - \cos(2\omega'_x t)}{2} \right. \quad (\text{B18})$$

$$\left. + (d-1) (\cos[(\omega'_x - \omega_x)t] - \cos[(\omega'_x + \omega_x)t]) \right]. \quad (\text{B19})$$

Taking the Gaussian average with $\mu = 0$ gives

$$\begin{aligned} \left([\text{Im}(K_d)]^2 P \right) (\omega_x) &= \frac{1}{d^2} \left[(d-1)^2 \frac{1 - e^{-2\sigma^2\omega_x^2}}{2} + \frac{1 - e^{-2\sigma^2\omega_x'^2}}{2} \right. \\ &\quad \left. + (d-1) \left(e^{-\frac{\sigma^2}{2}(\omega'_x - \omega_x)^2} - e^{-\frac{\sigma^2}{2}(\omega'_x + \omega_x)^2} \right) \right]. \end{aligned} \quad (\text{B20})$$

For $\omega_x \gg 1$ and $d > 2$, we obtain

$$\text{Var}_m[\text{Im}(h_d(E, x))] = \frac{(d-1)^2 + 1}{2d^2}, \quad (\text{B21})$$

recovering the same result obtained for the real part.

REFERENCES

-
- [1] Richard P. Feynman. Simulating physics with computers. *International Journal of Theoretical Physics*, 21(6):467–488, Jun 1982.
 - [2] David Deutsch. Quantum theory, the church-turing principle and the universal quantum computer. *Proceedings of the Royal Society of London. A. Mathematical and Physical Sciences*, 400(1818):97–117, 07 1985.
 - [3] E.M. Rains. Nonbinary quantum codes. *IEEE Transactions on Information Theory*, 45(6):1827–1832, 1999. <https://arxiv.org/abs/quant-ph/9703048>.
 - [4] D. Gottesman. Fault-tolerant quantum computation with higher-dimensional systems. *Chaos, Solitons and Fractals*, 10(10):1749–1758, September 1999. <https://arxiv.org/abs/quant-ph/9802007>.
 - [5] D. L. Zhou, B. Zeng, Z. Xu, and C. P. Sun. Quantum computation based on d-level cluster state. *Phys. Rev. A*, 68:062303, Dec 2003.
 - [6] Xiaoyang Shi, Jasmine Sinanan-Singh, Timothy J. Burke, John Chiaverini, and Isaac L. Chuang. Efficient implementation of a quantum algorithm with a trapped ion qudit. *Nature Communications*, 17(1):1911, Jan 2026.
 - [7] Michael Kues, Christian Reimer, Piotr Roztock, Luis Romero Cortés, Stefania Sciara, Benjamin Wetz, Yanbing Zhang, Alfonso Cino, Sai T Chu, Brent E Little, David J Moss, Lucia Caspani, José Azaña, and Roberto Morandotti. On-chip generation of high-dimensional entangled quantum states and their coherent control. *Nature*, 546(7660):622–626, June 2017.

- [8] Long B Nguyen, Noah Goss, Karthik Siva, Yosep Kim, Ed Younis, Bingcheng Qing, Akel Hashim, David I Santiago, and Irfan Siddiqi. Empowering a qudit-based quantum processor by traversing the dual bosonic ladder. *Nat. Commun.*, 15(1):7117, August 2024.
- [9] Clément Godfrin, Rafik Ballou, Edgar Bonet, Mario Ruben, Svetlana Klyatskaya, Wolfgang Wernsdorfer, and Franck Balestro. Generalized ramsey interferometry explored with a single nuclear spin qudit. *NPJ Quantum Inf.*, 4(1), October 2018. <https://arxiv.org/abs/1810.10367>.
- [10] Branislav Ilikj and Nikolay V. Vitanov. Ramsey interferometry with qudits, 2025.
- [11] Kenneth Choi, Dean Lee, Joey Bonitati, Zhengrong Qian, and Jacob Watkins. Rodeo algorithm for quantum computing. *Phys. Rev. Lett.*, 127:040505, Jul 2021. <https://arxiv.org/abs/2009.04092>.
- [12] Zhengrong Qian, Jacob Watkins, Gabriel Given, Joey Bonitati, Kenneth Choi, and Dean Lee. Demonstration of the rodeo algorithm on a quantum computer. *The European Physical Journal A*, 60(7), jul 2024. <https://arxiv.org/abs/2110.07747>.
- [13] R F I Gomes, J C S Rocha, W A T Nogueira, and R A Dias. Unraveling the rodeo algorithm through the zeeman model. *Physica Scripta*, 100(6):065119, may 2025. <https://arxiv.org/abs/2407.11301>.
- [14] Ashok Muthukrishnan C. R. Stroud. Quantum fast fourier transform using multilevel atoms. *Journal of Modern Optics*, 49(13):2115–2127, November 2002. <https://arxiv.org/abs/quant-ph/0112017>.
- [15] J.-L. Brylinski and Brylinski. *Universal quantum gates*, chapter 4, pages 117–134. Computational Mathematics. Chapman and Hall/CRC, 1 edition, 2002. <https://arxiv.org/abs/quant-ph/0108062>.
- [16] Gavin Brennen, Dianne O’Leary, and Stephen Bullock. Criteria for exact qudit universality. *Physical Review A*, 71(5), may 2005. <https://arxiv.org/abs/quant-ph/0407223>.
- [17] Noah Goss, Alexis Morvan, Brian Marinelli, Bradley K. Mitchell, Long B. Nguyen, Ravi K. Naik, Larry Chen, Christian J^onger, John Mark Kreikebaum, David I. Santiago, Joel J. Wallman, and Irfan Siddiqi. High-fidelity qutrit entangling gates for superconducting circuits. *Nature Communications*, 13(1):7481, Dec 2022.
- [18] J. Randall, S. Weidt, E. D. Standing, K. Lake, S. C. Webster, D. F. Murgia, T. Navickas, K. Roth, and W. K. Hensinger. Efficient preparation and detection of microwave dressed-state qubits and qutrits with trapped ions. *Phys. Rev. A*, 91:012322, Jan 2015.
- [19] Pranav Gokhale, Jonathan M. Baker, Casey Duckering, Natalie C. Brown, Kenneth R. Brown, and Frederic T. Chong. Asymptotic improvements to quantum circuits via qutrits. In *Proceedings of the 46th International Symposium on Computer Architecture*, ISCA ’19, page 554–566. ACM, June 2019.
- [20] Cao Ye, Peng Shi-Guo, Zheng Chao, and Long Gui-Lu. Quantum fourier transform and phase estimation in qudit system. *Communications in Theoretical Physics*, 55(5):790, may 2011.
- [21] Matthew Patkowski, Onat Ayyildiz, Katherine Hunt, Nathan Jansen, and Dean Lee. Improved rodeo algorithm performance for spectral functions and state preparation, 2026.
- [22] Francesco Pudda, Mario Chizzini, and Luca Crippa. Generalised quantum gates for qudits and their application in quantum fourier transform, 2024.
- [23] Mu He. The study on the kernel of series. *Journal of Physics: Conference Series*, 1168(5):052016, feb 2019.
- [24] J. C. S. Rocha, R. F. I. Gomes, W. A. T. Nogueira, and R. A. Dias. Estimating the number of states of a quantum system via the rodeo algorithm for quantum computation. *Quantum Information Processing*, 23(10), oct 2024. <https://arxiv.org/abs/2312.04322>.
- [25] Zeros of the Loschmidt amplitude correspond to nonanalyticities in the dynamical free energy, signaling dynamical quantum phase transitions (DQPTs) in the thermodynamic limit.
- [26] Since only entropy differences are thermodynamically relevant, the constant C may be safely neglected.
- [27] John Goold, Marcus Huber, Arnau Riera, Lidia del Rio, and Paul Skrzypczyk. The role of quantum information in thermodynamics, a topical review. *Journal of Physics A: Mathematical and Theoretical*, 49(14):143001, feb 2016.
- [28] D.H.E. Gross. *Microcanonical Thermodynamics: Phase Transitions in "small" Systems*. World Scientific lecture notes in physics. World Scientific, Singapore, 2001.
- [29] J. C. S. Rocha, R. A. Dias, and B. V. Costa. Microcanonical inflection-point analysis via parametric curves and its relation to the zeros of the partition function. *Phys. Rev. E*, 112:014112, Jul 2025. <https://arxiv.org/abs/2502.00999>.